Oxygen-induced $p(2\times3)$ reconstruction on Mo(112) studied by LEED and STM

T. Schroeder, J. B. Giorgi, A. Hammoudeh,* N. Magg, M. Bäumer,† and H.-J. Freund
Fritz-Haber-Institut der Max-Planck-Gesellschaft, Faradayweg 4 - 6, 14195 Berlin, Germany
(Received 12 July 2001; published 6 March 2002)

The open trough-and-row Mo(112) surface serves as substrate for the epitaxial growth of MoO_2. In the early stage of oxygen exposure, oxygen chemisorption induces a $p(2\times3)$ surface reconstruction of the missing row type on Mo(112). The surface structure of this reconstructed surface has been studied in detail by low-energy electron diffraction and scanning tunneling microscope. The experimental findings can be explained based on the effective medium theory for oxygen adsorption on transition-metal surfaces, providing a structure model for the oxygen-modified Mo(112) surface. The structure model allows the discussion of the oxygen-chemisorbed surface phase as a possible precursor state for the epitaxial MoO_2 growth on Mo(112).

DOI: 10.1103/PhysRevB.65.115411 PACS number(s): 68.35.Bs, 68.37.Ef, 68.47.Gh, 68.43.Fg

I. INTRODUCTION

Molybdenum and molybdenum oxides are used in many industrial catalysts for selective oxidation and hydrodesulfurization processes. This has encouraged the study of the dissociation and adsorption of oxygen, the oxygen-induced structures, and the oxide formation on the stable low-index Mo surfaces.[1–6] These studies include the (100), (110), and the (111) single-crystal surfaces.

Adsorption of oxygen on Mo(100) results in a consecutive series of ordered structures[7] of which the $(\sqrt{5}\times\sqrt{5})R(26°33')$ and the $p(2\times1)$ structure have been analyzed in detail by scanning tunnelling microscopy[8,9] (STM) and high-resolution electron-energy-loss spectroscopy.[10] In both cases, oxygen has been shown to occupy a threefold hollow site, resulting in the formation of an array of Mo_4O_4 clusters for the $(\sqrt{5}\times\sqrt{5})R(26°33')$ structure[7] and a missing-row reconstruction in case of the $p(2\times1)$ O-Mo(100) system.[10] Threefold hollow sites are also found to be the preferred adsorption sites in the $p(2\times2)$ O-Mo(110) system, and are reached at a coverage higher than 0.25 ML by site conversion from the long-bridge position.[11,12] This is different from the scenario on the Mo(111) surface where oxygen exposure results in the occupation of the threefold hollow sites from the beginning with additional on-top adsorbed oxygen detected at higher oxygen dosages.[13,14]

A first-principle calculation within the local-density functional formalism has been used recently to study the equilibrium crystal shape of molybdenum.[15] Beside the above mentioned (100), (110), and (111) orientations, the (112) single crystal surface is also remarkably stable and, therefore, found in the Wulff plot. A dynamical low-energy electron-diffraction (LEED) study of the Mo(112) surface revealed that the trough-and-row geometry with the lateral periodicity expected from the bulk material is conserved at the surface.[16]

To the best of our knowledge no systematic study of the oxygen adsorption behavior on the Mo(112) surface has been published up to now in the literature. This is surprising because the tendency of the open trough-and-row transition-metal surfaces to reconstruct under oxygen exposure exhibits a particularly rich surface chemistry that contributes much to our current understanding of the chemisorption and oxidation processes on transition-metal surfaces.[17,18] Among the most widely studied systems in this context are the trough-and-row Ag, Cu, Ni (110) (Ref. 19) and Co $(10\bar{1}0)$ surfaces (Ref. 20) of fcc and hcp crystals, respectively. In case of bcc crystals, such as, Mo, we are only aware of a diffraction study on the oxygen-exposed Fe(112) surface.[21]

In previous studies, the Mo(112) surface has been used by the authors of the present paper as substrate to set up the first successful preparation method for the growth of crystalline silicon dioxide films on a metal support.[22,23] To achieve an understanding as to which way the presence of the silica overlayer affects the surface chemistry of the substrate, we carried out a detailed multiple-technique study [x-ray photoemission spectroscopy (XPS)/ultraviolet photoemission spectroscopy (UPS)/infrared reflection absorption spectroscopy (IRAS)/STM/LEED] on the oxygen adsorption behavior of the Mo(112) surface. Here we monitored the gradual transformation of the clean Mo(112) surface under oxygen exposure into an epitaxially grown MoO_2 film.[24] In the early stage of oxygen chemisorption on the Mo(112) surface this transformation is found to proceed via an oxygen-induced surface reconstruction, which is discussed in this paper.

II. EXPERIMENT

The experiments in the present paper have been carried out in an Omicron multichamber UHV system with a base pressure of 2×10^{-10} mbar, described in detail elsewhere.[25] A self-designed high-temperature cell has been integrated to allow sample manipulation up to 2500 K. The high-temperature treatment is required to clean the Mo(112) surface. The cleaning procedure is described in the literature and consists of an oxidation step at 1500 K, followed by several high-temperature flashes to approximately 2300 K to free the surface from any residual molybdenum oxides.[26] Preparation of the $p(2\times3)$ O/Mo(112)-surface structure is carried out by exposing the clean Mo(112) surface at a temperature of 900 K to an oxygen dosage of approximately 1000 L (Langmuir). During the exposure the local oxygen pressure at the surface reaches a value of 3×10^{-6} mbar. No postannealing was applied after the exposure of the sample to oxygen. Sample transfer is carried out under UHV conditions for further sample characterization. The main chamber

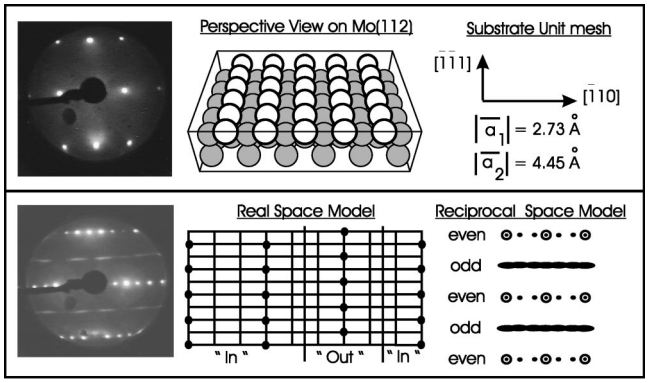

FIG. 1. *Upper panel*: LEED pattern ($E=56$ eV) and schematic structure for the clean Mo(112) surface. *Lower panel*: LEED picture ($E=56$ eV) and schematic models (reciprocal and real space) of the oxygen-added Mo(112) surface. Crystal orientation is given by the coordinate system together with the indexing of the axes.

is equipped with a four-grid LEED optics and a hemispherical electron energy analyzer (SES 200) for sample characterization by LEED and XPS/UPS studies, respectively. An Omicron VT-STM (variable-temperature scanning-tunneling microscope) chamber, attached to the same vacuum system, has been used for real-space studies of the surface in the constant current mode at room temperature.

III. RESULTS AND DISCUSSION

A. Reciprocal space information

Figure 1 summarizes the results of our LEED study for the clean (*upper panel*) and oxygen-modified Mo(112) surface (*lower panel*).

The clean Mo(112) surface exhibits a LEED pattern of rectangular symmetry, according to its unit mesh in real space. This can be inferred from the perspective view of the Mo(112) surface, where the surface is shown to consist of close-packed atomic rows that are oriented along the $[\bar{1}\bar{1}1]$ direction and are separated by furrows in the $[\bar{1}10]$ direction. According to the usual convention of x-ray crystallography, the indexing of the unit cell axis is chosen such that $|a_1| \leqslant |a_2|$.[27] The unit cell spacing along the close-packed atomic rows is 2.73 Å and across the troughs, the value is given by 4.45 Å.[28]

Exposing the clean Mo(112) surface to oxygen, under the conditions reported above, changes the LEED pattern substantially. A characteristic feature of the LEED pattern from the oxygen-modified Mo(112) surface is that, at a first glance, it appears to be a brilliant $p(1\times3)$ pattern. This points towards the formation of a perfect grating with three times the former substrate spacing along the $\mathbf{a}_2^*=[\bar{1}10]$ direction. A closer inspection of the pattern reveals the existence of less-intense spots situated at half the reciprocal unit vector spacing in the $\mathbf{a}_1^*=[\bar{1}\bar{1}1]$ direction. Therefore, after exposure to oxygen, the unit cell spacing along this direction is twice that of the clean Mo(112) surface. Due to the anisotropic broadening of these spots along the $\mathbf{a}_2^*$ direction, the smeared out intensity renders their detection difficult and the resolution of any further fine structure within those streaks impossible. In an earlier study from Fukui and co-workers, aiming at the modification of CO and H_2 adsorption on Mo(112) after oxygen exposure, these weak spots have not been reported.[29,30] Instead, these researchers only mention the observation of a $p(1\times3)$ phase by annealing at 700 K a $p(1\times2)$ oxygen-modified Mo(112) surface covered with excess oxygen.[29]

It is interesting to note that from the presence and orientation of these streaks in the LEED pattern of the oxygen-modified Mo(112) surface, valuable information can be gained about the surface defect structure. A sketch of the LEED pattern is shown in Fig. 1, where the rectangular Mo(112) substrate unit mesh is indicated by big circles, whereas, the overlayer is depicted by black dots and streaks. Counting from the (0,0) spot (center of the sketch) in the $\mathbf{a}_1^*=[\bar{1}\bar{1}1]$ direction reveals immediately that all even-order overlayer spots are sharp (black dots) and all odd-order superstructure spots are streaky (black streaks). Such periodic LEED patterns of sharp and streaky overlayer spots have been shown in the literature to arise whenever the long-range order of the surface structure is disturbed by the presence of antiphase domain boundaries.[31–33] For the oxygen-modified Mo(112) surface, this is shown in Fig. 1. The Mo(112) surface is represented by the rectangular unit mesh and the oxygen modification of the surface is indicated by a commensurate $p(2\times3)$ overlayer (black dots) with antiphase domain boundaries along the $[\bar{1}\bar{1}1]$ direction (black lines). It can be seen that in real space antiphase domain boundaries break the surface symmetry perpendicular to the domain boundary direction. This is the reason why antiphase domain boundaries with $[\bar{1}\bar{1}1]$ orientation in real space produce a spot broadening along the $[\bar{1}10]$ direction in reciprocal space. Furthermore, this spot broadening affects only odd-order spots in the broken symmetry direction because only for these an out-of-phase relationship results for the scattered intensity from adjacent domains. We can, therefore, conclude that the detected LEED pattern from the oxygen-added Mo(112) surface can be derived from a commensurate $p(2\times3)$ overstructure that is highly disordered by antiphase domain boundaries with $[\bar{1}\bar{1}1]$ orientation. However, due to the impossibility to resolve any fine structure within the very weak streaks in the LEED pattern of the oxygen-added Mo(112) surface, a $c(2\times6)$ instead of a $p(2\times3)$ parent phase with the same defect structure is also a possible explanation. Furthermore, from a kinematical LEED study alone, it is not possible to decide whether an ordered oxygen overlayer or an oxygen-induced reconstruction of the Mo(112) surface is the origin of the detected surface structure. To remove these uncertainties, a STM study has been carried out.

B. Real space information

The clean and oxygen-exposed Mo(112) surfaces have been studied at room temperature with atomic resolution using STM. The results of these studies are summarized in Fig. 2 and will be discussed in the following.

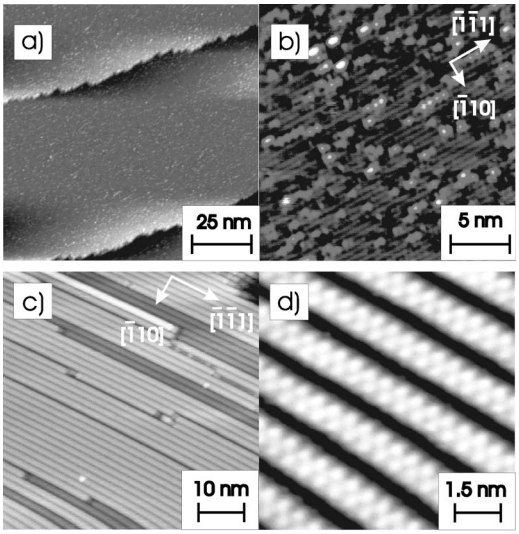

FIG. 2. *Upper horizontal row*: STM images of the clean Mo(112) surface (a) 100×100 nm^2 ($U_T=-1$ V; $I_T=4.5$ nA) and (b) 20×20 nm^2 ($U_T=-1$ V; $I_T=4.5$ nA). *Lower horizontal row*: STM images of the oxygen-added Mo(112) surface (c) 50×50 nm^2 ($U_T=-2.6$ V, $I_T=0.27$ nA) and (d) 7.5×7.5 nm^2 ($U_T=+2.6$ V, $I_T=0.1$ nA). Sample orientation is given within each row by the respective coordinate system.

1. The clean Mo(112) surface

STM topographs of the clean Mo(112) surface are shown in Figs. 2(a) and 2(b). According to a model calculation by Lang of the apparent size $\Delta s(U_T)$ of Mo atoms in STM images as a function of the applied bias U_T, a bias of $U_T=-1$ V has been chosen in the present study to maximize for the possible surface corrugation in the STM topographs.[34] The reason is that the calculated graph of $\Delta s(U_T)$ shows just a large peak at a value of $U_T=-1$ V tip bias associated with tunneling from the tip into the unoccupied, highly delocalized $5s$ states of the Mo sample atoms. In case of the reversed bias, there is only little evidence from this calculation that the tunnel current from the occupied Mo $4d$ valence states in the positively biased tip results in a detectable surface corrugation. This reflects the much smaller amplitude at the tip of the, in general, quite localized valence d orbitals relative to the valence s orbitals in the transition elements.

Figure 2(a) is an overview scan with a lateral extension of 100×100 nm^2 and shows substrate terraces with irregular steps in the $[\bar{1}\bar{1}1]$ direction. In general, however, no preferential direction for the terrace edges is detected. The terraces have an elongated form, extending over an average size of about 420 Å in the short direction and several 1000 Å in the long direction. Terraces are separated by steps with a height of about 1.2 or 2.4 Å. These step heights can be interpreted as single- and double-layer steps on the basis of the reported Mo(112) interlayer spacings derived by a dynamical LEED study.[16] A high-resolution scan of a sample area extending over 20×20 nm^2 is found in Fig. 2(b). The row-and-trough structure of the Mo(112) surface is clearly resolved and the unit cell spacing across the troughs and rows in the $[\bar{1}10]$ direction is thus visible. In this direction the detected surface corrugation is of the order of 0.1 Å, but much less along the close-packed rows in $[\bar{1}\bar{1}1]$ direction. Single atoms in the rows are, therefore, hard to visualize and we could not derive the Mo(112) unit cell spacing in the $[\bar{1}\bar{1}1]$ direction in our STM study. The Mo(112) terraces are rough on an atomic scale, showing protrusions and depressions of an apparent height and depth of about 0.6 and 0.3 Å, respectively. Having checked for surface cleanliness (absence of carbon and oxygen) by XPS, we interpret these protrusions and depressions in the STM image as Mo adatoms and Mo point defects on the Mo(112) terraces, respectively. This atomic scale surface roughness is found to increase substantially with higher cooling rates applied after the high-temperature flashes in the crystal cleaning procedure. STM studies on the Mo(112) surface require to control this parameter carefully. For the results reported here, point and adatom defect densities amount both to about 10% of a surface monolayer for the clean Mo(112) surface.

2. Oxygen-induced surface reconstruction on the Mo(112) surface

As pointed out in the Introduction, open transition-metal surfaces with trough-and-row surface structure are frequently found to reconstruct after (extensive) oxygen exposures.[18] Common, and therefore, characteristic features of the STM topographs from these orderly reconstructed O-metal (O-M) surfaces are greater protrusions, three to four times larger than the corrugation of the bare metals, the formation of unidimensional O-M-O chains and the presence/absence of missing rows.[35–37] The shape of the protrusions and the orientation of the O-M chains vary considerably from material to material and also from face to face. For example, the hcp trough-and-row surface Co$(10\bar{1}0)$ forms O-Co pairing chains in the $c(4\times2)$ O-Co$(10\bar{1}0)$ surface reconstruction, which are oriented *along the close-packed directions* and consist of protrusions of up to 1 Å height.[20] The resulting reconstructed phases after exposing the fcc trough and row (Ag,Ni,Cu) (110) surfaces to oxygen possess a high degree of similarity in the sense that they are all stabilized by single O-M-O strings. However, the O-M chains are running in these cases *perpendicular to the close-packed directions* in a so-called missing-row–added-row structure.[19] Finally for the bcc trough-and-row Fe(112) surface, a dynamical LEED study revealed a missing-row-type reconstruction in case of the $p(2\times1)$-O/Fe(112) surface phase where the O-M-O chains run *perpendicular to the close-packed substrate rows*.[21]

No STM study has been reported up to now on the oxygen reconstruction of bcc trough-and-row transition-metal surfaces. First STM topographs of such a study are shown in Figs. 2(c) and 2(d), which have been collected for the oxygen-added Mo(112) surface to complete the results of our LEED study. Figure 2(c) is an overview scan and shows that a well-ordered stripe structure exists on the surface that runs *along the close-packed substrate rows in the* $[\bar{1}\bar{1}1]$ *direction*. Perpendicular to the stripe orientation and along the

$[\bar{1}10]$ direction, the distance between single stripes corresponds to three times the former substrate unit cell spacing $3\times|a_2|=13.35$ Å. It is this well-developed $3\times|a_2|$ spacing between single stripes, extending over tens of nanometers along the $[\bar{1}10]$ direction, which builds up a perfect diffraction grating for electrons in our LEED study, giving rise to the brilliant $n\times1/3$ superstructure spots. In Fig. 2(d) it is seen that each of these stripes shows a fine structure. It is build up by strong protrusions, forming two rows that are staggered with respect to each other and run along the $[\bar{1}\bar{1}1]$ direction. Along this direction and within each row, the unit cell length of 5.46 Å detected by LEED appears in the STM images as the distance between adjacent protrusions.

We conclude that the key features in the STM images of the oxygen-modified Mo(112) surface (well-ordered stripe structure separated by depressions/protrusions much higher than on bare Mo) are in line with the above-mentioned characteristics of other STM studies carried out on oxygen-added transition-metal surfaces of trough-and-row geometry. Since for all these systems a surface reconstruction has been postulated and indeed confirmed for those that have been analyzed by diffraction techniques, an oxygen-induced surface reconstruction and *not* an ordered oxygen overlayer on an otherwise inert Mo(112) surface is likely to be at the origin of the studied O-Mo(112) system. It is interesting to note that recently a detailed angle-resolved ultraviolet photoemission spectroscopy study of the interplay between the Mo(112) surface band structure and possible surface reconstructions has been published.[38] In that study LEED and STM results show a (3×9) ''checkerboard'' and a (6×12) ''stripe'' structure surface reconstruction of the Mo(112) surface after exposure to less than 1 L (Langmuir) of carbon or oxygen.

3. Surface defect structure of the reconstructed Mo(112) surface

Figure 3 shows high-resolution scans of the oxygen-added Mo(112) surface where direction and position of the reported line scans are indicated by arrows. Beside the already discussed characteristic stripe structures running along the $[\bar{1}\bar{1}1]$ direction and consisting of two bright staggered rows of protrusions, we consider the resolution of a fine structure within the darker appearing depression lines *between* two neighboring stripes as the most important information in Fig. 3(a). Clearly Fig. 3(a) shows a further unidimensional protrusion line with $[\bar{1}\bar{1}1]$ orientation between two neighboring stripes, that is situated deeper in the surface. The internal characteristics of all these unidimensional protrusion lines (protrusion height and spacing) are the same, regardless of whether these protrusion lines form part of the stripes or are situated deeper in the depressions. As an example, a line scan over one of the stripe protrusion lines along the $[\bar{1}\bar{1}1]$ direction is shown. It shows a corrugation of about 0.4 Å between adjacent protrusions that are separated by a distance of twice the former substrate spacing $2\times|a_1|=5.46$ Å (vertical lines indicate the original substrate spacing). Therefore, it is the spacing between adjacent protrusions that sets the unit-cell spacing of the reconstructed surface in the $[\bar{1}\bar{1}1]$ direction.

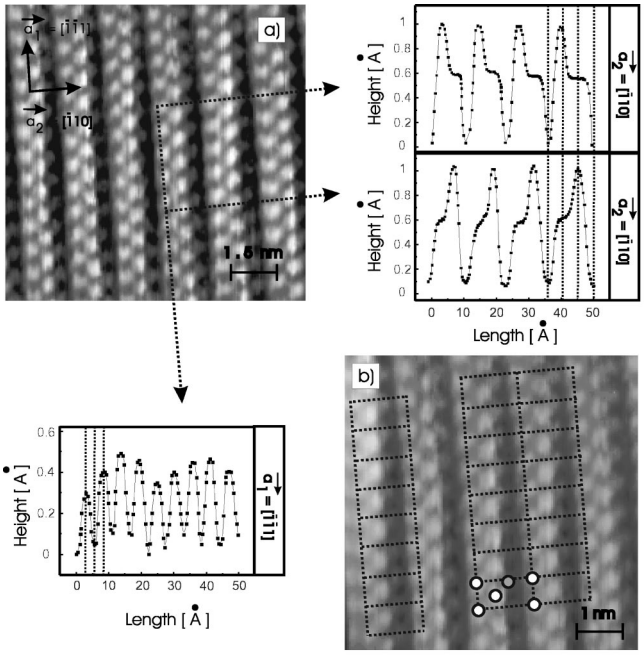

FIG. 3. (a) STM image (7.5×7.5 nm^2: $U_T=-0.55$ V; $I_T=0.5$ nA) with resolved stripe and depression structure. Crystal orientation is shown by the coordinate system and the arrows mark the direction and position of the presented line scans along the $[\bar{1}\bar{1}1]$ (left lower corner) and the $[\bar{1}10]$ (right upper corner) directions. Vertical lines in the line scan panels mark the original Mo(112) substrate spacing along the respective direction. (b) STM image (5×5 nm^2: $U_T=-0.55$ V; $I_T=0.5$ nA) with well ordered $p(2\times3)$ unit cells in the vicinity of an antiphase domain boundary, separating the left from the right unit-cell pile. Position of stripe and depression protrusions are visualized in one unit cell by white and gray balls, respectively.

Along the $[\bar{1}10]$ direction, the situation is more complicated due to the staggered arrangement of the protrusion lines with respect to each other. To account for this staggering, we show two line scans along the $[\bar{1}10]$ direction, which are shifted with respect to each other along the $[\bar{1}\bar{1}1]$ direction [Fig. 3(a)]. They differ from each other by the positions of their apices and shoulders. The top line scan in Fig. 3(a) runs over the left stripe protrusion lines (line scan apices). The elongated shoulders at the right side of the line scan apex belong to the depression protrusion line approximately 0.4 Å deeper in the surface. The bottom line scan passes over the right stripe protrusion lines (line scan apices) so that the left protrusion lines can just be seen as small shoulders to the left of the line scan apices. The dotted lines in these panels mark the former substrate unit cell spacing of $|a_2|=4.45$ Å. Beside the reconstructed unit-cell periodicity of $3\times|a_2|=13.35$ Å, we can derive a width of 4.45 Å for the prominent stripe structures. The latter results from the distance between the two staggered protrusion lines that set up the prominent stripes in the STM images (distance between the line scan apices in top and bottom line scan).

Furthermore, a maximum corrugation amplitude of about 1 Å is measured in these line scans between the apices and the points of deepest depression. The latter are found at a

distance of $|a_2|=4.45$ Å and $2\times|a_2|=8.9$ Å from a given line scan apex. This result is very interesting because it implies that the depression protrusion lines (seen as elongated shoulders in the upper line scan) cannot be situated at a position which corresponds to a close-packed substrate Mo row. Indeed, the depression protrusion line is found *closer*, i.e., at a distance of 2.4 Å and in a staggered position with respect to the nearest stripe protrusion line (distance between the elongated shoulder in top line scan and apex in the bottom line scan).

We conclude that the discussed line scans show a profile of the unit cell along the $[\bar{1}10]$ direction with a $3\times|a_2|=13.35$ Å periodicity. In this direction, the unit cell contains an entity of three parallel protrusion lines (running in the $[\bar{1}\bar{1}1]$ direction), which are all staggered with respect to each other: Two staggered protrusion lines with equal height build up the prominent stripe structures with a width of $1\times|a_2|=4.45$ Å, whereas, the third depression protrusion line is found 0.4 Å deeper in the surface. With a distance of 2.4 Å, it is found about 2 Å closer to its nearest stripe protrusion line than the original substrate spacing.

With these dimensions, a commensurate $p(2\times3)$ unit cell can be assigned to the STM image of the oxygen-reconstructed Mo(112) surface [Fig. 3(b)]. To guide the eyes, stripe and depression protrusions are sketched by white and gray balls, respectively. Long-range order of the $p(2\times3)$ unit cells in the $[\bar{1}\bar{1}1]$ substrate direction is well established by the $2\times|a_1|=5.46$ Å spacing and results in a perfect stacking of the unit cells along this direction. As for this $2\times|a_1|$ spacing two possible starting positions are offered by a substrate with $|a_1|$ spacing to start the unit-cell stacking in the $[\bar{1}\bar{1}1]$ direction, neighboring unit cell piles can be aligned [right part of Fig. 3(b)] or displaced by $1\times|a_1|$ [left part of Fig. 3(b)] along the $[\bar{1}10]$ direction with respect to each other. This kind of disorder introduces line defects running along the $[\bar{1}\bar{1}1]$ direction which break the surface symmetry along the $[\bar{1}10]$ direction. The STM Fig. 3(b) shows one such defect that (in the nomenclature of diffraction physics) is called an antiphase domain boundary. Defects of this kind have been postulated in Sec. III A to explain the odd-order spot streaking in the LEED pattern. In order to derive an estimate of the density of these line defects and quantify the size of the ordered domains on the $p(2\times3)$ oxygen-reconstructed Mo(112) surface, a spot profile analysis LEED study is required.

In conclusion, a $p(2\times3)$ oxygen induced surface reconstruction, disordered by antiphase domain boundaries running along the $[\bar{1}\bar{1}1]$ direction, appears to be the origin of the detected LEED pattern. The simultaneous presence of domains with $c(2\times6)$ unit cells is also in line with the results of our LEED study, but has not been detected in our STM study up to now.

4. A structure model of the p(2×3) O-Mo(112) surface reconstruction

Figure 4(a) summarizes all measured $p(2\times3)$ unit-cell coordinates, resulting from our STM study. Understanding the underlying real-space structure requires the assignment of a topological origin to the imaged features in the STM topographs. Combining STM and diffraction studies to analyze the oxygen-reconstructed fcc(110) surfaces revealed that the unidimensional chains of protrusions as the most common feature of the STM topographs from reconstructed O-metal surfaces correspond indeed to unidimensional O-M chains in real space.[19] The huge protrusions with corrugation three to four times higher than the bare metal surface, are attributed to metal-derived states from single atoms or clusters of metal atoms, whereas the minima in the corrugation correspond to a decrease in the amplitude of sample wave functions by a local increase of the sample work function due to oxygen sites. This interpretation of imaging the oxygen sublattice on metal surfaces as depressions in STM topographs seems to be widely accepted nowadays.[39] In a theoretical paper Doyen *et al.* predicted experimental conditions for which oxygen sites on a metal would appear as local maxima,[40] however, this was not confirmed by experimental work from the same group after studying ordered oxygen overlayers on a Ni(100) surface.[41]

Applying these concepts to the $p(2\times3)$-O Mo(112) system requires us to check experimentally the influence of the sample bias on the imaged features in the STM topographs. As can be seen from the different biases at which the selected STM images in Figs. 2 and 3 were collected, we found the observed features in the STM images to be widely bias independent. Therefore, we assign a topological origin to the detected protrusion chains along the $[\bar{1}\bar{1}1]$ direction and identify them with unidimensional O-Mo-O chains. Minima in the line scans along these stripe and depression protrusion lines with $[\bar{1}\bar{1}1]$ orientation correspond to oxygen sites separated by a distance of $2\times|a_1|=5.46$ Å. To establish a structure model, these minima must be identified with oxygen adsorption sites on the Mo(112) surface. The adsorption of oxygen on many low-index transition-metal surface shows the general tendency to take place in those adsorption sites where (a) the highest coordination number is found and where (b) the lowest degree of saturation of bonds exists.[18,42] These trends are discussed in detail in the framework of the effective medium theory (EMT) proposed by Stott and Zaremba[43] and Norskov and Lang.[17,44,45] Based on this approach we consider the hcp quasithreefold coordination sites on the Mo(112) surface composed of two row and one trough atom as the energetically most favored oxygen adsorption sites.

Figure 4(b) shows a side and top view of an oxygen-reconstruction model of the Mo(112) surface of the missing-row type. Along the $[\bar{1}10]$ direction, each third closed packed Mo row with $[\bar{1}\bar{1}1]$ orientation is missing. It is important to note that new oxygen adsorption sites of the proposed kind become available along the edges of the furrows created by the missing Mo rows. Oxygen atoms are distributed over these hcp quasithreefold coordination sites situated on two different height levels with a $2\times|a_1|$ spacing along the $[\bar{1}\bar{1}1]$ direction in such a way that (a) oxygen atoms saturate all low-coordinated Mo atoms by forming zigzag chains along the troughs and (b) without being forced to

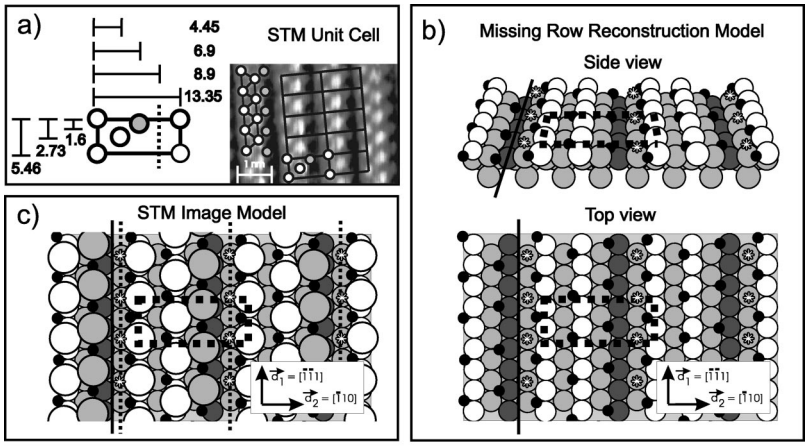

FIG. 4. (a) *Experimental unit-cell coordinates*: STM image with $p(2\times3)$ unit cells where one unit cell is shown with white and gray balls for stripe and depression protrusions, respectively. Left part of the images visualizes the zigzag pattern of one stripe structure by white balls. Unit cell sketch summarizes the dimension and coordinates within the unit cell (all values in Å; stripe and depression protrusion coordinates inaccurate by about 0.2 and 0.4 Å, respectively). Dashed vertical line shows the deepest depression line in the unit cell. (b) *Surface Reconstruction Model*: *Upper part of (b)* shows a perspective view of the oxygen reconstructed Mo(112) structure model of a missing-row type with a $p(2\times3)$ unit cell. Oxygen atoms in quasithreefold hollow sites and on-top positions are sketched as black spheres and black asterisks, respectively. First, second, and third layer Mo atoms appear as white, gray, and dark gray balls, respectively. An antiphase domain boundary is included and marked by a black line. *Lower part of (b)* shows a top view on this structure model. (c) *STM image model*: Top view of this structure model as viewed by STM. Protrusions in stripe and depression lines are created by two adjacent, not resolved metal atoms depicted by white and gray spheres of double size. The additional occupation of oxygen atoms in on-top positions (asterisks) along the $[\bar{1}11]$ direction raises the oxygen density so that STM detects these lines as the deepest depressions (dashed lines). A comparison of the resulting unit cell of the STM image model from part (c) with the detected STM unit cell in part (a) reveals the striking similarity.

share common low-coordinated Mo atoms. These oxygen atoms in hcp quasithreefold coordination sites are sketched by small black spheres in Fig. 4(b).

As a consequence of (a) the prominent stripe structures in the STM images with their internal zigzag pattern of staggered protrusions of the same height level arise. These are sketched in the STM image in Fig. 4(a) and in the STM image model in Fig. 4(c) by white balls. These zigzag first layer stripes can be traced back in the structure model in Fig. 4(b) to two adjacent first layer O-Mo-O chains, running along the $[\bar{1}11]$ direction and being staggered with respect to each other. Along the $[\bar{1}10]$ direction the measured stripe distance of $|a_2|=4.45$ Å is then a result of the Mo(112) substrate spacing $|a_2|$ between the two staggered O-Mo-O chains. Along the $[\bar{1}11]$ direction, protrusions and minima in each of these O-Mo-O chains at a spacing of $2\times|a_1|$ can now also be interpreted. Minima result from the adsorption of oxygen in only each second of the favored adsorption sites along the $[\bar{1}11]$ direction. In consequence, we find the protrusions in our model to be composed of two neighboring Mo atoms that appear unresolved in the STM images. Double-size spheres are, therefore, applied in the STM image model in Fig. 4(c) to sketch the protrusions, whereas the oxygen derived minima are depicted in the form of small black spheres.

The second criterion (b) not to force the oxygen atoms to share common low-coordinated Mo atoms is responsible for the $2\times|a_1|$ spacing along the $[\bar{1}11]$ direction. This idea results from many studies on oxygen adsorption on transition-metal surfaces[18] and an example is given by the appearance of the structure $c(4\times2)$-2O-Ru$(10\bar{1}0)$ before, at higher O coverages, Ru atoms are shared in the (2×1) $p2mg$-2O phase.[46] That oxygen atoms are not willing to do so before the O coverage is substantially increased, can again be understood in the EMT framework. Competition for the same charge density will force the oxygen atoms in search for the ''optimum'' charge density to approach closer to the surface that will raise the elastic lattice energy by distorting the adsorption site environment.

It is important to note that applying this criterion to the missing-row-type $p(2\times3)$-O Mo(112) system influences also the oxygen coverage along the edges of the furrows that are created by the missing first layer Mo rows. Adsorption sites of the proposed kind can only be occupied along one of the edges of these furrows since more adsorption would interfere with the oxygen atoms, which saturate all of the low-coordinated Mo atoms in the first layer rows [see Fig. 4(b)]. Further O-Mo-O chains along the $[\bar{1}11]$ direction at only one side of the furrow edges are created this way and have the same characteristics as the stripe protrusion lines, but are situated deeper in the surface. These depression protrusion lines are sketched in the STM image in Fig. 4(a) and the STM image model in Fig. 4(c) by gray spheres. The proposed structure model gives an explanation why STM detects the depression protrusion lines at a distance of just 2.4 Å from the nearest stripe protrusion line and, therefore,

closer than expected from the former substrate spacing $|a_2| = 4.45$ Å. Furthermore, it is interesting to note that the Mo atoms from the second, unoccupied furrow edge are only in part in contact with oxygen atoms that saturate all of the low-coordinated Mo atoms from the adjacent first layer rows. To saturate these undercoordinated second layer Mo atoms, additional oxygen atoms are adsorbed in on-top sites [asterisks in Fig. 4(b)]. The additional occupation of oxygen atoms in on-top positions raises the oxygen density along the second layer Mo rows situated at this site of the furrow edges. Accordingly, the region of these furrow edges should appear as strong depression in the STM images. This is indeed observed in the STM study because line scans along the $[\bar{1}\bar{1}1]$ direction in this region [indicated by the dashed line in Fig. 4(a)] show the deepest depression within the unit cell (minima in the line scans along the $[\bar{1}10]$ direction in Fig. 3) and do not reveal any substantial corrugation. Therefore, the structure model succeeds to explain the result of the STM study that the two furrow edges of the missing Mo rows are inequivalent. This is best seen in the upper line scan along the $[\bar{1}10]$ direction in Fig. 3. Between the line scan minimum and maximum, the depression protrusion line appears as a shoulder to the left of the minimum, whereas to the right, just a sharp transition towards the line scan maximum occurs.

To summarize, the proposed structure model succeeds in reproducing the unit cell spacings as well as the unit cell content, as can be seen by comparison of the unit cell in our STM image model in Fig. 4(c) with the detected STM unit cell in Fig. 4(a). Roughly speaking and without taking possible small distortions into consideration, the $2\times|a_1|$ spacing is found to correspond to the oxygen spacing along the $[\bar{1}\bar{1}1]$ direction, whereas the $3\times|a_2|$ dimension in the $[\bar{1}10]$ direction is due to each third Mo row missing. Given the strong difference in the form factors and, therefore, the electron scattering strength of oxygen and Mo atoms, the structure model also accounts for the detected intensity difference between the superlattice spots in the LEED pattern. The brilliant $p(1\times3)$ structure in the LEED pattern results from the $3\times|a_2|$ missing row supergrating set up by the strongly scattering Mo surface. The weak superlattice spots at halfway along the reciprocal $[\bar{1}\bar{1}1]$ unit-cell dimension are due to the $2\times|a_1|$ supergrating produced by the weakly scattering oxygen atoms. Furthermore, these spot intensities are smeared out as a result of the detected antiphase domain boundaries running along the $[\bar{1}\bar{1}1]$ direction.

The presence of these line defects and their orientation is in line with the present structure model. The important point is that these defects do not increase the epitaxial interface energy. No change in the O-M and M-M bond balance is required to produce this misalignment between $p(2\times3)$ unit cells along the $[\bar{1}10]$ direction. This is shown in the sketch of our structure model [Fig. 4(b)] where such an antiphase domain boundary is depicted and marked by a black line. Completely different is the situation along the $[\bar{1}\bar{1}1]$ direction where we find the lines of protrusion to be perfectly evolved and nearly free of defects. In our structure model, an interruption of this one-dimensional O-M chains results in an increase in the number of M-M bonds at the cost of M-O bonds. This is equivalent to saying that the metal coordination number increases for the metal atoms at such a defect. That a lowering and not an increase of the metal coordination number is favorable for an increase in bonding strength between the regarded metal atom and neighboring oxygen atoms has been explained within the framework of EMT theory.[17] Lowering the metal coordination number by breaking metal-metal bonds causes an upward shift of the metal *d* band with respect to the Fermi level. As these metal *d* states become the antibonding part in the O-M interaction, less occupation of antibonding states increases the crystal orbital overlap population and results in stronger bonding. This electronic energy contribution is also the main driving force for reconstructions to occur on transition-metal surfaces after oxygen adsorption. Whenever this energy gain outweights the cost of breaking metal-metal bonds (what is easier to achieve for open surfaces), oxygen chemisorption induces a surface reconstruction of the transition-metal surface.[19]

IV. CONCLUSION AND OUTLOOK

Through the combination of LEED and STM results, the presented surface crystallographic study of oxygen chemisorption on the Mo(112) surface clearly shows that a $p(2\times3)$ oxygen-induced surface reconstruction of the missing-row type precedes the formation of an epitaxial MoO_2 layer on Mo(112). Based on the results of the effective medium theory, we present a structure model for the reconstructed surface, which is in line with all our experimental findings, i.e., the unit cell dimensions and the surface defect structure in the form of antiphase domain boundaries running along the $[\bar{1}\bar{1}1]$ direction. A good starting point is thus set for a future quantitative dynamical LEED analysis to resolve the surface structure exactly.

It is very tempting to elucidate the way the MoO_2 lattice evolves out of this surface reconstruction. The monoclinic MoO_2 lattice can be derived from the tetragonal rutile structure through a small distortion that conserves the trigonal coordination sphere of the oxygen atoms and the octahedral environment of molybdenum, but introduces a metal-metal dimerization between edge-sharing octahedra along the crystallographic *c* axis.[47] The central idea is to align this *c* axis of the MoO_2 lattice with the densely packed Mo rows along the $[\bar{1}\bar{1}1]$ direction of the Mo(112) substrate. This can be achieved by a (100) and/or (010) orientation of the MoO_2 lattice with respect to Mo(112). Both structures fit within 8% to the Mo(112) substrate spacings and seem, therefore, possible candidates for the MoO_2 epilayer. It is interesting to note that RuO_2 is found to grow with (100) orientation on the trough-and-row Ru$(10\bar{1}0)$ surface structure[48] where oxygen adsorption has been proven to take place in the here-postulated threefold hcp adsorption sites.[46] If the situation for the MoO_2 growth on Mo(112) is similar, then the here-studied oxygen-induced surface reconstruction of the Mo(112) surface can indeed be regarded as a precursor state of the MoO_2 lattice. The surface reconstruction provides the

trigonal coordination sphere of the oxygen atoms in the MoO_2 lattice in the form of the hcp adsorption sites. The Mo-Mo dimer formation along the *c* axis in MoO_2 evolves probably out of the unidimensional protrusion chains along the $[\bar{1}11]$ direction where our structure model interprets each protrusion to be composed of two neighboring Mo atoms, remaining unresolved in the STM images (see Fig. 4). A STM study is under way to check these ideas.[24]

We wish to acknowledge the valuable assistance of Dr. H. Over and Dr. U. Starke from the Fritz-Haber-Institute in dealing with the topics of oxygen chemisorption on transition-metal surfaces. J.B.G. and N.M. would like to thank, respectively, the Alexander von Humboldt Foundation and the Studienstiftung des Deutschen Volkes for financial support. In addition, we are grateful to the following agencies for financial assistance: Deutsche Forschungsgemeinschaft (DFG), Bundesministerium für Bildung und Forschung (BMBF), Fonds der Chemischen Industrie, and NEDO (International Joint Research Grant on Photon and Electron Controlled Surface Processes).

*Present address: Department of Chemistry, Yarmouk University, P.O. Box 566, Irbid, Jordan.

†Corresponding author. Email address: baeumer@fhi-berlin.mpg.de

[1] I. A. Toyashima and G. A. Somorjai, Catal. Rev. - Sci. Eng. **19**, 19 (1979).

[2] Y. Iwasawa, Adv. Catal. **35**, 187 (1987).

[3] N. Floquet and O. Bertrand, J. Solid State Chem. **93**, 96 (1991).

[4] K. T. Queeney and C. M. Friend, J. Chem. Phys. **109**, 6067 (1998).

[5] G. Mestl and T. K. K. Srinivasan, Catal. Rev. - Sci. Eng. **40**, 451 (1998).

[6] C. M. Friend, K. T. Queeney, and D. A. Chen, Appl. Surf. Sci. **142**, 99 (1999).

[7] I. K. Robinson, D.-M. Smilgies, and P. J. Eng, J. Phys.: Condens. Matter **4**, 5845 (1992).

[8] H. Xu and K. Y. Simon Ng, Surf. Sci. **355**, L305 (1996).

[9] H. Xu and K. Y. Simon Ng, Surf. Sci. **356**, 19 (1996).

[10] S. H. Kim and P. C. Stair, Surf. Sci. **457**, L347 (2000).

[11] J. Kröger, S. Lehwald, and H. Ibach, Phys. Rev. B **58**, 1578 (1998).

[12] J. Kröger, T. Greber, and J. Osterwalder, Surf. Sci. **459**, 173 (2000).

[13] Ts. S. Marinova, P. K. Stefanov, and N. Neshev, Surf. Sci. **164**, 196 (1985).

[14] P. K. Stefanov and Ts. S. Marinova, Surf. Sci. **200**, 26 (1988).

[15] J. G. Che, C. T. Chan, W.-E. Jian, and T. C. Leung, Phys. Rev. B **57**, 1875 (1998).

[16] D. Kolthoff, H. Pfnür, A. G. Fedorus, V. Koval, and A. G. Naumovets, Surf. Sci. **439**, 224 (1999).

[17] J. Norskov, Rep. Prog. Phys. **53**, 1253 (1990).

[18] H. Over, Prog. Surf. Sci. **58**, 249 (1998).

[19] F. Besenbacher and J. K. Norskov, Prog. Surf. Sci. **44**, 5 (1993).

[20] R. Koch, E. Schwarz, K. Schmidt, B. Burg, K. Christmann, and K. H. Rieder, Phys. Rev. Lett. **71**, 1047 (1993).

[21] J. Sokolov, F. Jona, and P. M. Marcus, Europhys. Lett. **1**, 401 (1986).

[22] T. Schroeder, M. Adelt, B. Richter, M. Naschitzki, M. Baumer, and H.-J. Freund, Microelectron. Reliab. **40**, 841 (2000).

[23] T. Schroeder, M. Adelt, B. Richter, M. Naschitzki, M. Bäumer, and H.-J. Freund, Surf. Rev. Lett. **7**, 7 (2000).

[24] T. Schroeder, J. B. Giorgi, N. Magg, M. Bäumer, and H.-J. Freund (unpublished).

[25] M. Frank, Ph.D. thesis, Humboldt-Universität Berlin, 2000.

[26] R. G. Musket, W. McLean, C. D. Colmenares, D. M. Makowiecki, and W. J. Siekhaus, Appl. Surf. Sci. **10**, 143 (1982).

[27] G. Ertl and J. Kueppers, *Low Energy Electron Diffraction and Surface Chemistry*, 2nd ed. (VEB Chemie, Weinheim, 1985).

[28] O. M. Braun and V. K. Medvedev, Sov. Phys. Usp. **32**, 328 (1989).

[29] K. Fukui, T. Aruga, and Y. Iwasawa, Surf. Sci. **281**, 241 (1993).

[30] T. Aruga, K. Tateno, K. Fukui, and Y. Iwasawa, Surf. Sci. **324**, 17 (1995).

[31] A. J. C. Wilson, *X-Ray Optics*, 2nd ed. (Mathuen, London, 1962).

[32] J. Libuda, F. Winkelmann, M. Bäumer, H.-J. Freund, Th. Bertrams, H. Neddermeyer, and K. Mueller, Surf. Sci. **318**, 61 (1994).

[33] J. Wollschläger, J. Falta, and M. Henzler, Appl. Phys. A: Solids Surf. **A50**, 57 (1990).

[34] N. D. Lang, Comments Condens. Matter Phys. **14**, 253 (1989).

[35] C. Q. Sun and C. Bai, J. Phys. Chem. Solids **58**, 903 (1997).

[36] C. Q. Sun, Appl. Phys. Lett. **72**, 1706 (1998).

[37] C. Q. Sun and S. Li, Surf. Rev. Lett. **7**, 213 (2000).

[38] T. McAvoy, J. Zhang, C. Waldfried, D. N. McIlroy, P. A. Dowben, O. Zeybeck, T. Bertrams, and S. D. Barrett Eur. Phys. J. B **14**, 747 (2000).

[39] J. Wintterlin, J. Trost, S. Renisch, R. Schuster, T. Zambelli, and G. Ertl, Surf. Sci. **394**, 159 (1997).

[40] G. Doyen, D. Drakova, E. Kopatzki, and R. J. Behm, J. Vac. Sci. Technol. A **6**, 327 (1988).

[41] E. Kopatzki and R. J. Behm, Surf. Sci. **245**, 255 (1991).

[42] P. M. Marcus, J. E. Demuth, D. W. Jepsen, Surf. Sci. **53**, 501 (1975).

[43] M. J. Stott and E. Zaremba, Phys. Rev. B **22**, 1564 (1980).

[44] J. K. Norskov and N. D. Lang, Phys. Rev. B **21**, 3037 (1980).

[45] J. K. Norskov, Phys. Rev. B **26**, 2875 (1982).

[46] S. Schwegmann, A. P. Seitsonen, V. De Renzi, H. Dietrich, H. Bludau, M. Gierer, H. Over, K. Jacobi, M. Scheffler, and G. Ertl, Phys. Rev. B **57**, 15 487 (1998).

[47] V. Eyert, R. Horny, K.-H. Hock, and S. Horn, J. Phys.: Condens. Matter **12**, 4923 (2000).

[48] Y. D. Kim, S. Schwegmann, A. P. Seitsonen, and H. Over, J. Phys. Chem. B **105**, 2205 (2001).